Research Article Vol. 5, No. 7 / July 2018 / Optica 793



Quantum dot white LEDs with high luminous efficiency

Sadra Sadeghi,[1,†] Baskaran Ganesh Kumar,[2,4,†] Rustamzhon Melikov,[2] Mohammad Mohammadi Aria,[3] Houman Bahmani Jalali,[3] and Sedat Nizamoglu[1,2,3,*]

[1]Graduate School of Materials Science and Engineering, Koç University, Istanbul 34450, Turkey
[2]Department of Electrical and Electronics Engineering, Koç University, Istanbul 34450, Turkey
[3]Department of Biomedical Sciences and Engineering, Koç University, Istanbul 34450, Turkey
[4]Current address: Department of Chemistry, PSR Arts and Science College, Sivakasi, India
*Corresponding author: snizamoglu@ku.edu.tr

Received 22 February 2018; revised 29 May 2018; accepted 30 May 2018 (Doc. ID 324694); published 12 July 2018

Colloidal quantum dots (QDs) have attracted significant attention in the last three decades due to high quantum yield (QY) and tunable electronic properties via quantum confinement effect and material composition. However, their utilization for efficient solid-state lighting sources has remained a challenge due to the decrease of QY from the synthesis batch in the liquid state to the host matrix in the solid state, which is also known as the host material effect. Here, we suppress the host material effect by simple liquid-state integration in light-emitting diodes (LEDs) that lead to a luminous efficiency of 64 lm/W for red, green, blue (RGB)-based and 105 lm/W for green, blue (GB)-based white light generation. For that, we maximized the QY of red- and green-emitting QDs by optimizing synthesis parameters and integrated efficient QDs with QY up to 84% on blue LED dies in liquid form at appropriate injection amounts for high-efficiency white lighting. Liquid-state integration showed two-fold and six-fold enhancement of efficiency in comparison with incorporation of QDs in polydimethylsiloxane film and close-packed formation, respectively. Our theoretical calculations predicted that the luminous efficiency of liquid QD-LEDs can reach over 200 lm/W. Therefore, this study paves the way toward ultra-high-efficiency QD-based lighting. © 2018 Optical Society of America under the terms of the OSA Open Access Publishing Agreement

OCIS codes: (160.4236) Nanomaterials; (230.3670) Light-emitting diodes; (160.2540) Fluorescent and luminescent materials; (250.5590) Quantum-well, -wire and -dot devices; (250.5230) Photoluminescence.

https://doi.org/10.1364/OPTICA.5.000793

1. INTRODUCTION

Efficient solid-state lighting (SSL) offers a high potential for saving energy and protecting the environment [1]. If light-emitting diodes (LEDs) at the targeted efficiency levels are replaced with conventional lighting sources, the global electricity that is consumed for lighting would be decreased by more than 50%, which is equal to the reduction of either 230 typical 500-MW coal plants or 200 million tons of greenhouse gas emission [1,2]. According to the SSL road map, white LEDs were targeted to reach a luminous efficiency (LE) level over 200 lumen per electrical watt until 2020 [3]. To this end, there is a significant worldwide effort to boost the efficiency levels of white LEDs.

Today, white LEDs generally use a down-conversion material that is integrated on a blue LED die in a solid-state matrix [1,4]; instead, the synergetic combination of fluids and optics, which is also known as optofluidics, may open up new horizons due to its ability to reveal novel and advanced functionalities [5–9]. Photonic materials in the liquid state advantageously enable simple integration. In addition, the optical properties of the fluid medium can be changed by replacing it with another one, and the spectra can be adjusted by controlling the blend ratio of the fluids. Hence, photonic materials in the liquid state facilitated significant progress in displays, lasers, energy storage, and wave guiding [10–13]. Furthermore, there have been previous reports that use liquid-state photonic materials on LEDs for spatial radiation control [14], color mixing [15], and flexible electronics [16], and they have recently started to be explored as an alternative for efficient lighting [17,18].

Colloidal quantum dots (QDs) have attracted significant attention for efficient lighting due to high quantum yield (QY > 80%), narrow emission bandwidth, and tunable luminescence [19–25]. Even though QDs have many advantageous features for LEDs, the efficiencies that have been achieved so far were not at the desired levels, mainly due to host material effect and reabsorption [26–28]. To overcome this limitation, giant shell growth on a core facilitated the preservation of QY from solution to polymer matrix in addition to suppressing the self-absorption [27,29,30]. However, the QY of these structures was less than 50%, and the emission could only cover the red spectral region. Alternatively, recycling of trapped excitons via energy transfer is

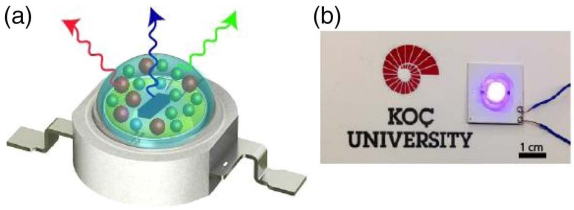


Fig. 1. (a) Schematic of the LQD-LED. The red and green spheres represent red- and green-emitting QDs in a liquid, respectively. QDs absorb the blue electroluminescence and emit red and green light. The combination of red and green emission by QDs and blue emission by a blue LED die generates white light. (b) Photograph of an exemplary white LQD-LED, while it is turned on.

another effective way to increase the in-film quantum efficiencies (QEs). It was demonstrated that by using this approach, the in-film QE can be increased [31], which can be also used for LEDs as well [32]. But, since QE in a close-packed formation drastically decreases, it cannot be recovered close to its original levels. Moreover, dispersion of the colloidal QDs while transferring from liquid to solid (e.g., inkjet printing [33]) generates undesirable inhomogeneity due to the coffee ring effect [34]. Therefore, liquid-state integration can generate a solution for the above-mentioned problems.

Here, in this study, we integrated QDs in a liquid state on blue LED chips for efficient lighting [Fig. 1(a)]. The electroluminescence of the blue LED chip excites the QDs in liquid, which generate photoluminescence (PL), and the joint electroluminescence of blue LED and PL of QDs form the white light [Fig. 1(b)]. For that, we optimized the QY of red- and green-emitting Cd-based QDs by varying the synthesis parameters. The integration of QDs in a liquid state enables the preservation of QY. We integrated as-synthesized liquid QDs without any chemical or interfacial modification and injected at appropriate injection amounts, which led to the most efficient QD-based white LED reported to date, according to our best of knowledge.

2. METHODS AND MATERIALS

A. Synthesis of Red-Emitting CdSe/CdS/ZnS Core/Shell/Shell Quantum Dots

CdSe/CdS/ZnS quantum dots were synthesized based on the method by Lim *et al.* [35]. In a typical synthesis, 0.4 mmol cadmium oxide (0.0515 g, >99.99% Aldrich), 1.6 mmol oleic acid (0.5 ml, 99% Alfa), and 5 ml tri-n-octylamine (>97%TCI) were mixed together in a 100 ml three-neck round-bottom flask. The solution was heated to 150°C under a nitrogen inert atmosphere. At this temperature, the solution was evacuated by vacuum and placed under an inert atmosphere repeatedly. After the degassing process, the solution was heated to 300°C. Once the temperature was stable, 0.05 ml of 0.792 g selenium (>99.5% Aldrich) in a trioctylphosphine (90% Acros) precursor (2M TOPSe) was injected into the solution. After 2 min, 1.5 ml of 210 μl 1-octanethiol (>98.5% Aldrich) in a 6 ml TOA precursor was injected into the solution in 90 s. The heating continued for 40 min until the reaction was complete. Then, 4 ml of 0.92 g zinc acetate (>99.0% Sigma-Aldrich) in a 3.15 ml oleic acid (OA) (100°C, transparent) precursor (0.25M Zn-OA) was injected into the solution for 2 min. Quickly after this injection, 1.75 ml of 1.12 ml 1-octanethiol (6.4 mmol) in a 6 ml TOA precursor was injected into the solution for 105 s. Finally, the solution was cooled down to room temperature. The final red solution consisted of red-emitting CdSe/CdS/ZnS quantum dots, which was purified with ethanol and re-dispersed in toluene.

B. Synthesis of Green-Emitting CdSe//ZnS/CdSZnS Core/Shell Quantum Dots

CdSe//ZnS/CdSZnS quantum dots were synthesized based on the method by Jang *et al.* [24,36]. In a typical synthesis, 0.4 mmol CdO (0.0515 g), 0.8 mmol of octadecylphosphonic acid (0.268 g, >98% TCI), and 16 ml of TOA were mixed together in a 100 ml three-neck flask. The solution was heated to 150°C under a nitrogen inert atmosphere. At this temperature, the solution was evacuated by vacuum and placed under an inert atmosphere repeatedly. After the degassing process, the solution was heated to 320°C under a nitrogen atmosphere. Once the temperature was stable, 1 ml of 0.792 g Se in a TOP precursor (2M TOPSe) was injected into the solution. After 2 min of reaction time, the heating was stopped and the mantle was removed. The synthesized core CdSe quantum dots were purified, centrifuged, and re-dispersed in toluene. The optical density of the ×100 times diluted core solution was adjusted at 0.1 at the first absorption maximum. Then, 0.4 mmol of zinc acetate dihydrate (0.088 g) was mixed with 0.8 mmol of OA (252 μl) and 16 ml TOA in a three-neck round-bottom flask. The mixture was heated to 150°C under a nitrogen inert atmosphere. At this temperature, the solution was evacuated by vacuum and placed under inert atmosphere repeatedly. After the degassing process, the solution was heated to 320°C under a nitrogen atmosphere. Once the temperature was stable, 1 ml of the core solution was injected into a zinc-containing solution. Right after injection, 1.6 mmol of 1-octanethiol (278 μl) in 2 ml TOA was injected into the solution incrementally. The heating was continued for 40 min. The synthesized CdSe//ZnS interfused quantum dots were purified and re-dispersed in toluene. The CdSZnS shell was formed according to the procedure in Ref. [24]. 0.05 mmol cadmium acetate (0.0115 g, ≥ 99.995% Aldrich), 0.04 mmol zinc acetate (0.0088 g), and 1.5 mol OA (480 μl) was dissolved in 20 ml TOA in a round-bottom flask. The mixture was heated to 150°C under a nitrogen inert atmosphere. At this temperature, the solution was evacuated by vacuum and placed under inert atmosphere repeatedly. After the degassing process, the solution was heated to 320°C under a nitrogen atmosphere. Once the temperature was stable, 0.6 ml of the core CdSe//ZnS solution with optical density of 0.15 was injected into the Cd-and-Zn-containing solution. Right after the injection, 2 ml of 0.4 M sulfur (reagent grade 100 mesh particle size, Sigma-Aldrich) in TOP was injected into the solution incrementally. The heating continued for 45 min. The synthesized CdSe//ZnS/CdSZnS quantum dots were purified with ethanol and re-dispersed in toluene. Each synthesis for optimization of the QY for both red- and green-emitting QDs was performed three times to assure the reproducibility of the results.

C. Instrumentation and Characterization

Powder X-ray diffraction (XRD) measurements of red-emitting CdSe/CdS/ZnS QDs and green-emitting CdSe//ZnS/CdSZnS QDs were performed by Bruker D2 PHASER *X*-ray diffractometer [$\lambda_{\text{Cu-K}\alpha} = 1.54$Å] with 1°min^{-1} scan rate. Powder samples were prepared by drying the QD solution dissolved in hexane.

The drying process was carried out by heating the solution to 200°C for 1 h. Powder samples were supported by a polymethyl methacrylate (PMMA) holder, and the studies were carried out at room temperature. Ultraviolet (UV)/visible absorption and the PL spectra of the QDs were carried out by an Edinburgh Instruments Spectrofluorometer FS5 with a 150 W xenon lamp combined with an excitation monochromator. The excitation wavelength was 375 nm with a band pass filter with a full width at half-maximum (FWHM) of 2 nm. Standard quartz cuvettes were used for absorbance and PL spectroscopy. The emission detector was a single photon counting photomultiplier tube (R928P). Absolute fluorescence quantum yield values were measured by using an integrating sphere module in FS5. The measurement module contained an integrating sphere with an inner diameter of 150 mm, which was placed into the FS5 system for the determination of quantum yields. Scanning electron microscopy energy dispersive spectroscopy (SEM EDS) measurements were obtained by a Zeiss Ultra Plus field emission scanning electron microscope by using a Bruker XFlash 5010 EDX detector. The accelerating voltage was set to 20 kV. The samples were prepared by drying the QDs dissolved in hexane solution to 200°C for 1 h. The transmission electron microscopy (TEM) was performed using a Fei Talos F200S 200 k microscope with an accelerating voltage of 200 keV. The dried QDs are also probed by X-ray Photoelectron Spectroscopy (XPS) via a Thermo Scientific K-Alpha spectrometer using an aluminum anode (Al $K\alpha =$ 1468.3 eV) at an electron take-off angle of 90° (between the sample surface and the axis of the analyzer lens). The spectra were recorded using an Avantage 5.9 data system. The binding energy scale was calibrated by assigning the C1s signal at 284.5 eV.

D. Lens Making Procedure

For making the semi-spherical lens, 1 g of Polydimethylsiloxane (PDMS) SYLGARD 184 Elastomer was mixed with 0.1 g of SYLGARD 184 curing agent and stirred for 3 min until bubbles appeared in the mixture. Then, the mixture was degassed in the vacuum desiccator for 20 min until the bubbles disappeared completely. The mixture was poured into the pre-fabricated aluminum mold and heated at 70°C for 6 h for completion of the PDMS curing process. After heating was finished, the aluminum mold was opened and the lens was brought out. The product was a semi-spherical lens with outer diameter of 9 mm and inner diameter of 7 mm and lens thickness of 1 mm.

E. LED Device Making Procedure

For making the LED device, the blue chip was mounted on a board, and two electrical wires were soldered to the board for connection to the voltage supply. As a step-wise curing process, the PDMS lens was attached to the LED printed circuit board (PCB) with a NOA 68 UV curable polymer. The UV curable polymer was dripped on the sides of the lens, and it was cured for 20 min in front of UV irradiation at 365 nm. This process was repeated two times to assure that the structure was leakage proof.

F. LED Measurements

For LED measurement, a EP-B4040F-A3 InGaN/GaN 350 mA blue LED chip from Secol Company with an illumination wavelength at 455 nm was used. The chips were mounted on a PCB board. LED measurements were performed with a multi-port Ocean Optics integrating sphere. The detector was an Ocean Optics Torus with optical resolution of 1.6 nm FWHM over the spectra range, integration time from 4 ms to 10 s, and the wavelength range was from 300 to 900 nm. The signal-to-noise ratio was 250:1. The luminous efficiency was calculated based on [37].

G. Fabrication of Close-Packed- and Solid-State LEDs

As a close-packed-state LED, UV curable polymer was mounted around the blue chip to prevent the liquid from moving to the board edge. 10 μl of red-emitting QDs solution with an optical density of 0.033 and 120 μl of green-emitting QDs solution with an optical density of 0.048 (the same amounts used for the RGB LQD-LED) was mixed and poured on top of the blue chip to dry. For the solid-state LED, 10 μl of red-emitting QDs solution with an optical density of 0.033 and 120 μl of green-emitting QDs solution with an optical density of 0.048 was mixed with a 250 μl SYLGARD 184 Elastomer and a 50 μl SYLGARD 184 curing agent. The mixture was degassed and cured at 70°C for 6 h. Each structure was fabricated and measured three times to assure the reproducibility of the results.

3. RESULTS AND DISCUSSION

A. Quantum Yield Optimization of Red- and Green-Emitting Quantum Dots

Since the QY of the synthesized QDs directly affects the overall performance of the LEDs, it is critical to synthesize QDs with a high QY. In this study, we used "/" for separation between core/shell structures, and "//" to indicate the interfused structure. For red-emitting QDs, the synthesis starts with the CdSe core. Since the core QY directly affects the QY of the core/shell structures, different selenium precursor injection temperatures have been investigated to observe the effect of temperature on QY of the synthesized CdSe core QDs. For this purpose, selenium was injected into the Cd-containing solution (1:1 molar ratio) at reaction temperatures of 220°C, 240°C, 260°C, 280°C, 300°C, and 320°C [see Fig. 2(a)]. As the temperature increased, the QY increased, and the CdSe core showed the highest value of 38% at 300°C after 2 min reaction time [Fig. 2(a)].

In principle, there were also other alternative QD reaction times and temperatures that have high efficiency (e.g., QY of 35% at 260°C in 7 min or QY of 37% at 240°C in 60 min) (see Fig. S1, Supplement 1). However, we selected the CdSe core at 300°C with 2 min of reaction time due to the position of the PL peak wavelength, which will experience wavelength shift after shell growth and could reach an appropriate final wavelength for efficient white light generation. On the CdSe core, the CdS shell with a low lattice mismatch of 4.3% was grown, which facilitates the reduction of trapped states [38]. To find the optimum point, the reaction proceeded up to 60 min, and aliquots were taken at different CdS growth times [Fig. 2(b)]. The highest QY was observed as 56% after 40 min of CdS shell growth on the CdSe core. After the growth of the CdS shell, the FWHM did not change considerably (i.e., 28 nm for CdSe and 31 nm for CdSe/CdS in Fig. S2 of Supplement 1), which indicated the homogenous size distribution of the synthesized QDs after shelling. Finally, the ZnS shell was grown for strong confinement of both the electron and the hole inside the QDs. We optimized the final heterostructure by varying the CdS and ZnS shells (Fig. S3, Supplement 1), and the structure with only one shelling of

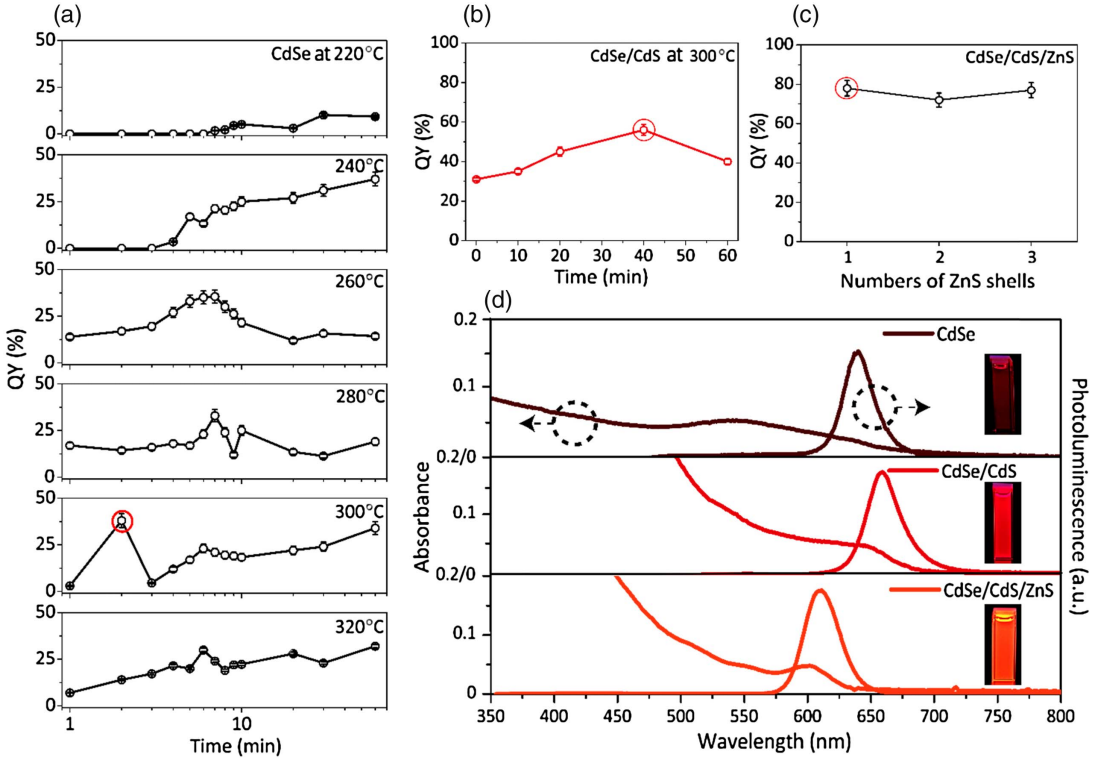


Fig. 2. (a) Optimization of the QY of the CdSe core by modifying the temperature and time. (b) Optimization of the QY of the CdSe/CdS core/shell QDs by varying the reaction time at 300°C. (c) Effect of multiple ZnS shelling on the QY of CdSe/CdS/ZnS core/shell/shell QDs. (d) Absorbance and photoluminescence spectra of CdSe (upper panel), CdSe/CdS (middle panel) and CdSe/CdS/ZnS (lower panel) QDs at the optimized reaction time and temperatures. Inset: photograph of the QD solutions at each step under 365 nm UV radiation. The optimized operating points were placed in solid red circles ($n = 3$).

CdS and ZnS showed the highest QY of 77% [Fig. 2(c)]. The progress in absorbance and PL spectra of CdSe core, CdSe/CdS, and CdSe/CdS/ZnS QDs were shown in Fig. 2(d). The PL peak wavelengths of the synthesized red-emitting QDs were 640 nm, 659 nm, and 609 nm for CdSe, CdSe/CdS, and CdSe/CdS/ZnS, respectively [Fig. 2(d)].

Similarly, we investigated the synthesis procedure of green-emitting CdSe//ZnS/CdSZnS core/shell QDs to maximize the QY. CdSe core investigation was re-performed because of using a different surfactant, which is a mixture of octadecylphosphonic acid (ODPA) and OA, and the synthesis showed the highest QY of 17% at 320°C [Fig. 3(a)]. Afterward, an interfused CdSe//ZnS core formation was generated, which showed a significant blue shift from CdSe QDs PL peak wavelength from 526 to 501 nm [Fig. 3(b)] due to the larger bandgap of CdSe//ZnS in comparison with CdSe. After 40 min, the interfused core showed the maximum QY of 51% [Fig. 3(c)]. CdSZnS shell synthesis on the core for 45 min caused a significant boost of QY from 51% to 84% [Fig. 3(d)]. At the same time, the CdSZnS shell favorably resulted in a significant red-shift in PL peak wavelength from 501 to 550 nm with a FWHM of 35 nm [Fig. 3(b)], which is in the close proximity of the peak of eye-sensitivity function (at 555 nm) to achieve efficient white LEDs.

The structural analysis of the synthesized QDs was investigated by using TEM (Fig. S4, Supplement 1). The synthesized red- and green-emitting QDs showed a size distribution of 6.23 ± 0.77 nm and 5.89 ± 0.93 nm, respectively (Fig. S4, Supplement 1). Moreover, the SEM EDS measurement also confirmed the presence of cadmium, selenium, zinc, and sulfur in red- and green-emitting QDs (Fig. S5, Supplement 1). The cubic structures of the synthesized red- and green-emitting QDs were identified by XRD (Fig. S6, Supplement 1). The peaks at 25°, 28°, 42°, and 57° confirmed the CdSe, CdS, and ZnS structures (Fig. S6, Supplement 1). At the same time, XPS measurement showed the core/shell structures of the red- and green-emitting QDs (Fig. S7, Supplement 1).

B. Simulation of Optical Properties of the Generated White Light

To achieve the highest level of efficiency in color conversion, it is necessary to optimize the injection ratio (concentration) of red- and green-emitting QDs. For this purpose, we initially simulated external quantum efficiency (EQE) of single-type red- and green-emitting QDs at different optical densities. The solid lines in Figs. 4(a) and 4(b) showed the theoretical EQE of the QDs in liquids, and according to the simulation, they need to drop due to the reabsorption losses. Experimentally, we also confirmed this behavior as well; as the optical density of red-emitting QDs increased from 0.0033 to 0.2, the EQE decreased from 76.7% to 61.2%, respectively. The same behavior was also observed for green-emitting QDs in which by increasing the optical density from 0.0026 to 0.2, the EQE of the QDs decreased from 83.9% to 77.6%, respectively. Furthermore, the spectrum of the liquid-state QDs also shifted, while the optical density varied. As the optical density increased toward 0.2, the FWHM of the red-emitting QDs increased from 32 to 36 nm in Fig. 4(c).

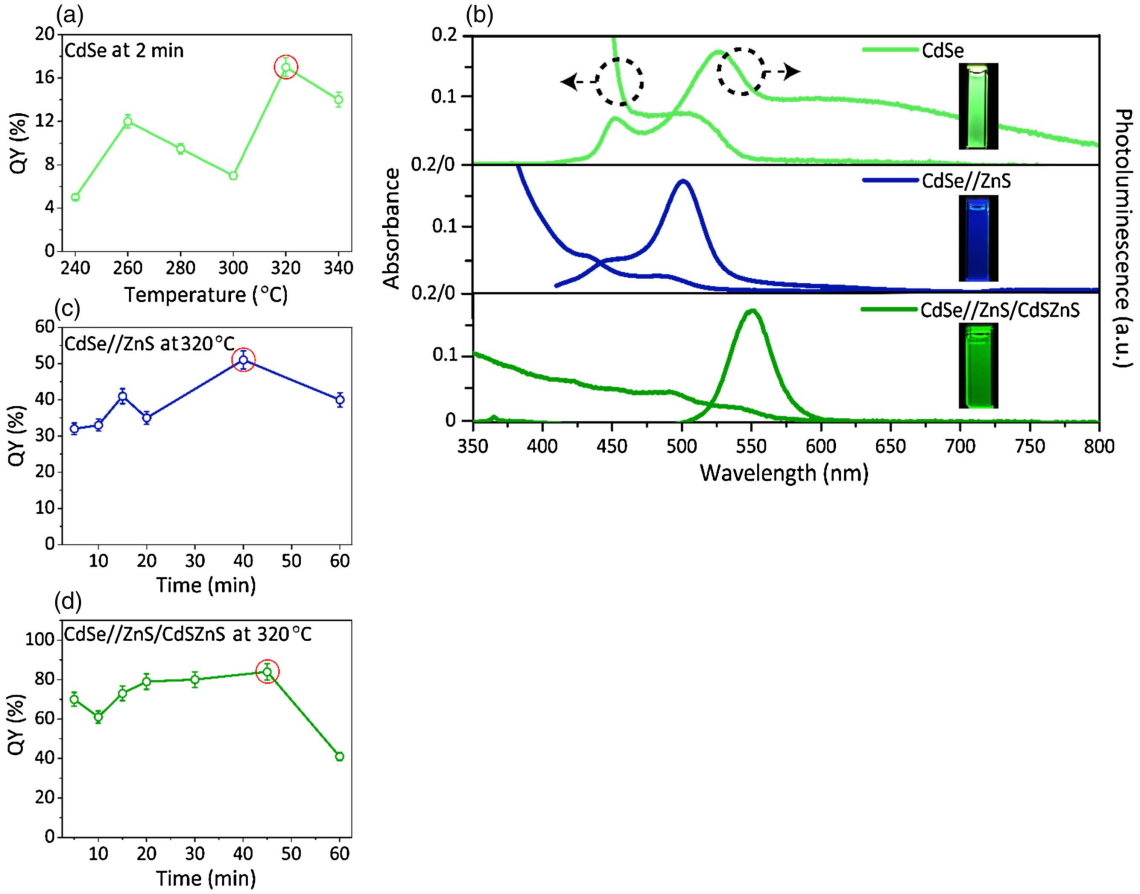


Fig. 3. (a) Optimization of QY of green-emitting CdSe core QDs by changing the temperature at 2 min reaction time. (b) The absorbance and photoluminescence spectra of optimized CdSe core (upper panel), CdSe//ZnS core (middle panel), and CdSe//ZnS/CdSZnS core/shell (lower panel) QDs. Inset: photograph of the QD solutions at each step under 365 nm UV radiation. (c) Optimization of QY of CdSe//ZnS interfused core QDs by varying the reaction time at 320°C. (d) Optimization of QY of CdSe//ZnS/CdSZnS QDs by modifying CdSZnS shelling reaction time at 320°C. The optimized operating points were placed in solid red circles ($n = 3$).

Moreover, the PL peak wavelength of the red-emitting QDs was red-shifted 8 nm (from 610 to 618 nm) [Fig. 4(c)]. Similarly, the FWHM of green emission increased from 36 to 37 nm accompanied by a peak wavelength change from 550 to 553 nm, which was also in agreement with the simulations. According to these analyses, it is necessary to take the reabsorption-originated spectral and efficiency shift into account to achieve efficient lighting. Therefore, the injection optical density of red- and green-emitting QDs needs to be optimized. To explore the possible injection ratios that may lead to high-efficiency LEDs, we investigated the single and double combinations of red- and green-emitting QDs on a blue LED die [see Figs. 4(e) and Supplement 1 for a detailed explanation about the simulation]. First, our simulation showed that the injection amounts need to be carefully adjusted that could lead to (x, y) tristimulus coordinates in the white region. By considering an optical density range [0,0.1] and [0,1] for red- and green- emitting QDs, respectively, the white light region covered only ~5% of the total possible combinations (Fig. S8, Supplement 1). Second, we calculated that liquid-state integration with 77% and 84% QY of red- and green-emitting QDs could reach a maximum LE of 112 lm/W for white light generation on a blue die with an EQE of 50% [Fig. 4(f)], while the device-originating losses such as the refractive index mismatch, total internal reflection, waveguiding effect, and other possible optical loss mechanisms were considered in our simulation by an approximate factor ($\eta = 0.77$) [39]. If red- and green-emitting QDs were synthesized with a QY of 100%, the maximum achievable LE would reach 140 lm/W by using a blue LED die with EQE of 50% [Fig. 4(f)]. At the same time, the simulation results showed that if the state-of-the-art blue LED die with EQE of 85% was used [40] with the red- and green-emitting QDs that have a QY of 100%, the LE would reach over 200 lm/W [Fig. 4(f)].

C. Liquid-State Integration of Quantum Dots onto Blue LED Die

For liquid-state integration, we fabricated a LED structure that held a QD solution on top of the blue LED die. We prepared a transparent PDMS polymeric lens [Fig. 5(a)] that was mechanically stable and that could recover its surface against the needle holes after the injection (see Fig. S9 of Supplement 1 and Section 2 (Methods) for a detailed explanation of lens curing). The main advantage of a PDMS lens is its scalability for mass production due to its quick production time and low cost [41]. In addition, the light extraction can be sensitively controlled by changing the lens design from a semi-sphere to flat lens geometry. We placed the lens on top of the blue LED chip [in Figs. 5(b) and 5(c)-left], and the polymeric lens and the LED chip board were adhered together by a commercial UV curable polymer

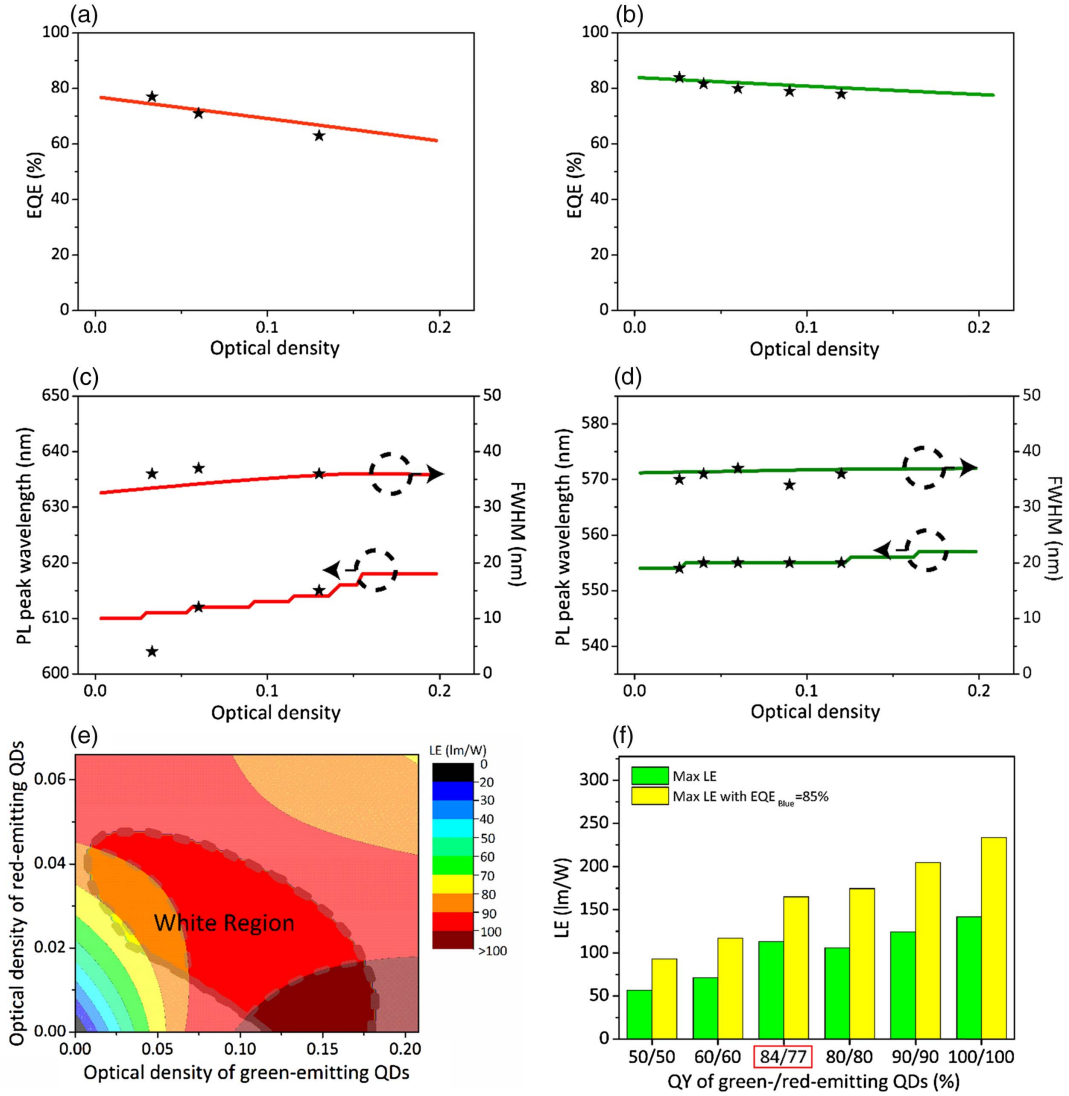


Fig. 4. EQE of (a) red-emitting CdSe/CdS/ZnS and (b) green-emitting CdSe//ZnS/CdSZnS QDs at different optical density levels. The photoluminescence peak position and FWHM of (c) red-emitting CdSe/CdS/ZnS and (d) green-emitting CdSe//ZnS/CdSZnS QDs at different optical density levels. The star symbols show the experimentally measured data points, and the solid lines show the theoretically simulated data points. (e) Counter plot of luminous efficiency with the combinations of red- and green-emitting QDs at different optical density levels ($\eta = 0.77$). White color coordinates were shown as the dashed bright region (white region). (f) Luminous efficiency simulation results for different QYs of red- and green-emitting QDs illuminated with a blue LED pump with EQE = 50% (i.e., max LE) and 85% (i.e., max LE with EQE = 85%) while $\eta = 0.77$.

and cured for stabilization of the lens on top of the board [Fig. 5(c)-middle]. Afterward, a QD solution was injected into the PDMS polymer lens by using a typical micro-syringe [Figs. 5(c)-right and 5(d)]. To check the functionality of the hybrid LED device, red-emitting CdSe/CdS/ZnS and green-emitting CdSe//ZnS/CdSZnS QD solutions were injected into the device, respectively, and white light generation was observed while the LED was turned on [Fig. 5(e)].

For display application, we injected red- and green-emitting QDs with optical densities of 0.033 and 0.048 on a blue LED die at 455 nm, respectively (see Fig. S10 in Supplement 1 for the detailed characterization of the blue LED die). The total emission spectrum that was generated by the QDs and LED die was shown in Fig. 5(f). The generated white light corresponded to (x, y) tristimulus coordinates of (0.31, 0.32) in a CIE 1931 color gamut with a luminous efficacy of optical radiation (LER) of 368 lm/W and a color correlated temperature (CCT) of 6298 K. The LE of the white LED was measured as 64 lm/W (see Fig. 5(j) [24,42,43–56]). By mixing the synthesized QDs with phosphorous, it is also possible to achieve high LE [57]. The intensity spectra of white LED at different injection currents from 10 to 150 mA were shown in Fig. 5(g), and the (x, y) tristimulus coordinates remained with small changes ($\Delta x = 0.002$, $\Delta y = 0.003$) in the white region due to non-photoluminescence-saturation of the QDs at higher injection currents. Furthermore, the functionality of the RGB LQD-LED was tested in the display panel in Fig. 5(h). Two manufactured white LQD-LEDs were used as a backlight in a LCD TV, and the LQD-LEDs led to bright and vivid images. Moreover, the EQE of the LQD-LEDs was measured during time to assess the photostability up to 100 h [Fig. 5(i)]. The measured effective EQE at different time intervals, which was calculated by dividing luminous efficiency to luminous efficacy

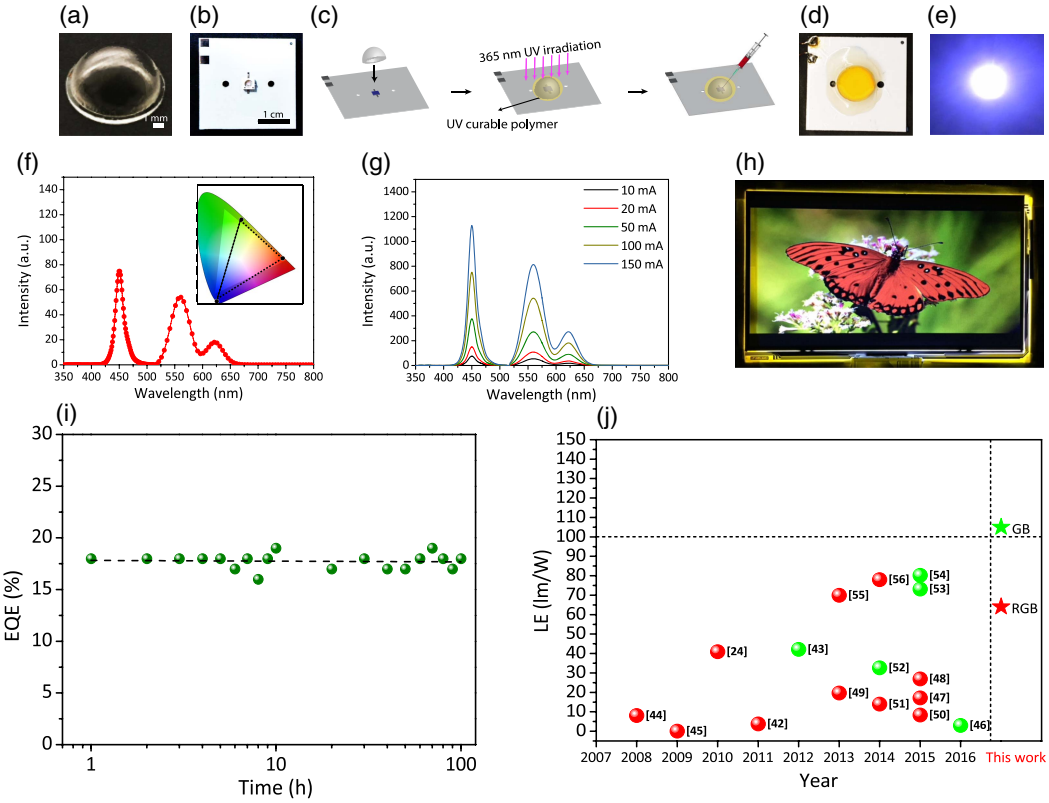


Fig. 5. (a) PDMS polymeric lens. (b) Blue LED die on the board. (c) Schematic of the fabrication process. The PDMS lens was placed on top of the chip and adhered via UV curable polymer with 365 nm UV irradiation. Afterward, red- and green-emitting QDs were injected into the lens. (d) Photograph of LQD-LED under ambient light. (e) Photograph of LQD-LED when it was turned on. (f) Spectrum of the white LQD-LED. Inset: the black dashed triangle shows the color gamut in CIE 1931 color coordinates. (g) White LED spectra at different injection currents from 10 to 150 mA. (h) Photograph taken from a display illuminated by two white LQD-LEDs that were used as backlights in a 7-inch LCD TV. (i) Optical stability of the LQD-LEDs after 100 h illumination. (j) LE of the previous reports that use QDs as the only color converter. The red and green colors refer to dual- and single-type quantum dot combinations for white LEDs, respectively. The red and green stars correspond to our dual- (RGB) and single-type (GB) quantum dot combinations for white LEDs, respectively.

of optical radiation (LE/LER) [58], confirmed the stability of LQD-LEDs, which showed its potential for long-term applications. In addition to its high efficiency, liquid-state integration of QDs can be advantageous in terms of stability. It can prevent the elevation of LED temperature, especially at higher injection currents [15]. According to the theoretical analysis, the use of green-emitting QDs on a blue LED could generate an efficiency level above 100 lm/W, if they were injected at an optical density range in between 0.1 and 0.2. To further boost the LE, we injected green-emitting QDs at a concentration of 0.13 on a blue LED die, which led to a green, blue (GB)-based white LED with a record performance of 105 lm/W [green star symbol in Fig. 5(j), and see Fig. S11 of Supplement 1 for properties of a GB white LED].

Since QDs have narrow emission linewidths (~35 nm) in comparison with inorganic phosphors (~100 nm), they can be spectrally optimized to match the color filter spectra in LCDs by using a combination of the narrow emitters for display application, which can simultaneously result in both a high color gamut and LE. According to our simulation (Code 1, Ref. [59]), while sweeping the peak wavelengths by 5 nm steps and using the parameters of the optimized QDs (see Tables S1 and S2 in Supplement 1), a maximum possible color gamut of 104% (Fig. S12, Supplement 1) or a maximum LE of 120 lm/W (Fig. S13, Supplement 1) is achievable. Moreover, for lighting applications, our simulations showed that the highest color rendering index (CRI) value of 84 with LE of 80 lm/W is achievable by using the optimized green- and red-emitting QDs (Fig. S14, Supplement 1).

D. Comparison of Liquid-State, Solid-State, and Close-Packed-State Quantum Dot White LEDs

The performance of the LQD-LED was compared with a close-packed QD-LED and a solid-state QD-LED that was made of QDs in a PDMS polymer matrix (see Section 2 (Methods) for a detailed explanation of the preparation). In all the device architectures, the total amount of QDs was kept fixed, and Figs. 6(a) and 6(b) showed OFF and ON states of the close-packed- and solid-state QD-LEDs, respectively. For the close-packed QD-LED, the QDs were dried on top of the blue chip and they showed aggregation and cracks in the film, which resulted in less green and red color conversion [Fig. 6(c)]. This led to an undesirable (x, y) tristimulus point of (0.19, 0.07) outside the white region [Fig. 6(c)-inset], and aggregation also induced a significant reduction of the efficiency with a LE of only 11 lm/W [as shown in Fig. 6(e)]. While the QDs were in a polymer matrix, this resulted in an effective color conversion [Fig. 6(d)], which had an (x, y) point of (0.35, 0.37) in the white region with a CCT of 4812 K [Fig. 6(d)-inset]. However, the solid-state QD-LED

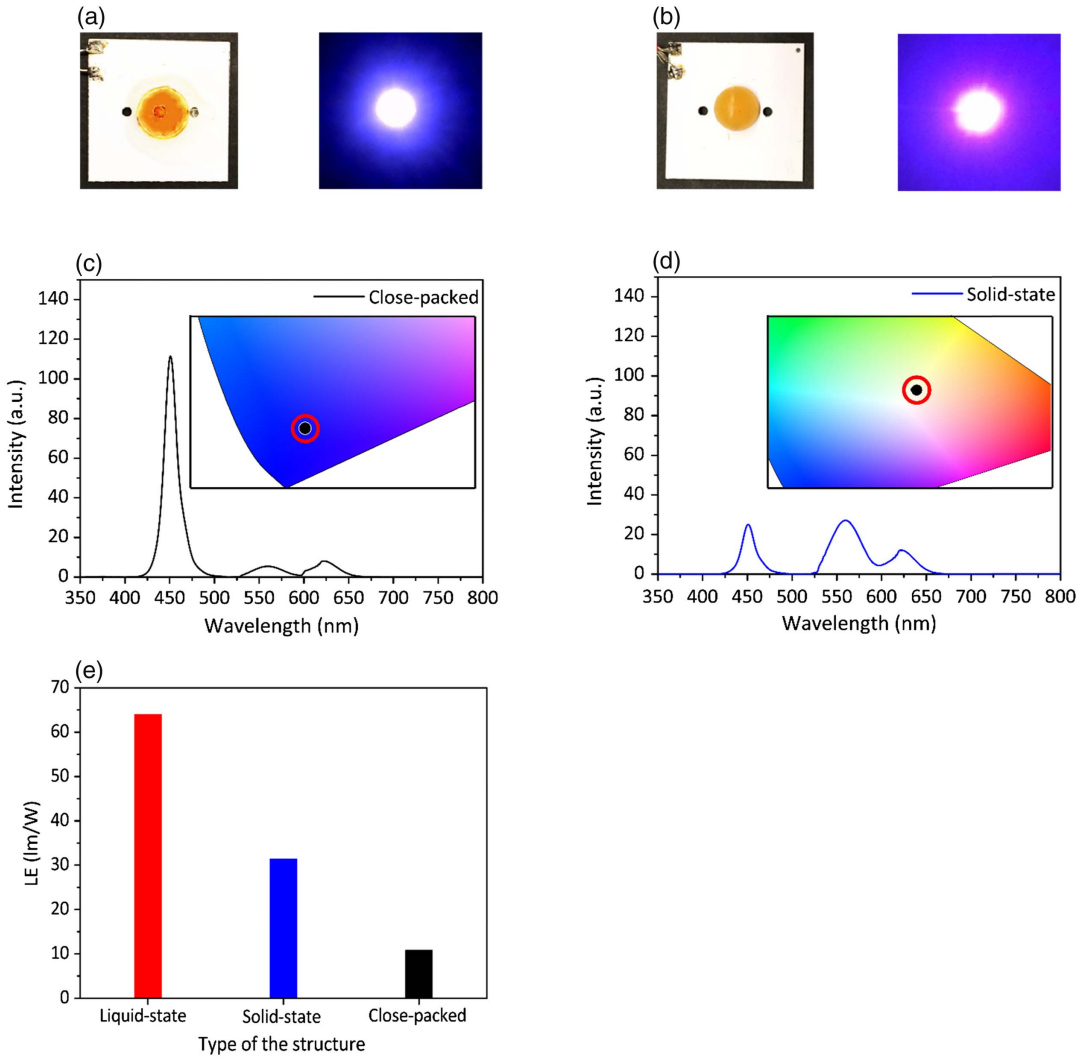


Fig. 6. (a) Photograph of close-packed QD-LED when it was turned OFF under ambient light (left) and turned ON (right). In this close-packed QD-LED configuration, QDs were directly dried on top of the blue LED die. (b) Photograph of solid-state QD-LED when it was turned OFF under ambient light (left) and turned ON (right). In the solid-state QD-LED configuration, QDs were dispersed and cured in a PDMS polymeric matrix on top of a blue LED die. (c) The spectrum of the close-packed QD-LED at a current injection level of 10 mA. Inset: (x, y) tristimulus coordinates of the close-packed QD-LED. (d) Spectrum of the solid-state QD-LED at a current injection level of 10 mA. Inset: (x, y) tristimulus coordinates of the close-packed QD-LED. (e) LE of all the QD-LEDs at a current injection level of 10 mA.

showed an LE of 31 lm/W [as shown in Fig. 6(e)] due to the host material effect. Comparatively, the LQD-LED showed the highest LE of 64 lm/W due to keeping their high efficiency in liquid form [see Fig. 6(e)]. The optical properties of the liquid-state, solid-state, and close-packed QD-LEDs at different injection currents were shown in Fig. S15, Supplement 1.

4. CONCLUSION

In conclusion, there were critical factors that were satisfied to achieve high-performance QD-integrated white LEDs. First, high-efficiency LEDs were achieved by the liquid-state integration, which significantly increased the luminous efficiency even more than 50% due to suppressed host material effect. Second, as the QY of the QDs increased, the number of emitted photons to the absorbed photons enhanced significantly, which resulted in a more efficient color conversion and consequently higher efficiency of the white LEDs. Third, the color converted spectra were fine-tuned to keep the peaks close to the peak of the eye sensitivity function, which led to high luminous efficacy of the optical radiation and simultaneously luminous efficiency as well. Moreover, minimization of the other losses such as using blue LED chips with higher EQE, refractive index matching, and using a back reflector can directly boost the performance levels reported within this study. In addition, our theoretical calculations showed that the combination of state-of-the-art blue LED die with an EQE of 85% and red- and green-emitting QDs with a QY of unity has the potential to exceed the level of 200 lm/W, which was targeted by the SSL road map until 2020. Therefore, we believe that liquid-state integration of QDs holds great promise for efficient white LEDs, and after quantum dot TVs in the market, we may see them in the near future in lighting as well.

Funding. Türkiye Bilimsel ve Teknolojik Araştirma Kurumu (TüBITAK) (114E194, 114F317, 115E115, 115E242, 115F451);

Marie Curie Career Integration (PROTEINLED, 631679); Türkiye Bilimler Akademisi.

Acknowledgment. We thank Dr. Daniel Aaron Press for LED discussions. We sincerely thank Dr. Ceren Yilmaz Akkaya for XRD and Dr. Baris Yagci for SEM EDS and XPS measurements at KUYTAM (Koç University Surface Science and Technology Center). We gratefully acknowledge Prof. Funda Yagci Acar for fluorescence spectroscopy measurements and Prof. Ismail Lazoglu and Muzaffer Butun for their support on fabrication of the aluminum mold for lens fabrication. We sincerely thank Hasan Can and Central Research Laboratory at the University of Bayburt for TEM measurements. We sincerely thank Prof. Mehmet Arik and Enes Tamdogan at Ozyegin University.

See Supplement 1 for supporting content.

†These authors contributed equally to this work.

REFERENCES

1. S. Pimputkar, J. S. Speck, S. P. DenBaars, and S. Nakamura, "Prospects for LED lighting," Nat. Photonics **3**, 180–182 (2009).
2. M. R. Krames, O. B. Shchekin, R. Mueller-Mach, G. O. Mueller, L. Zhou, G. Harbers, and M. G. Craford, "Status and future of high-power light-emitting diodes for solid-state lighting," J. Disp. Technol. **3**, 160–175 (2007).
3. J. Y. Tsao, *Light Emitting Diodes (LEDs) for General Illumination* (Optoelectronics Industry Development Association, 2002), pp. 289–290.
4. Q. Sun, Y. A. Wang, L. S. Li, D. Wang, T. Zhu, J. Xu, C. Yang, and Y. Li, "Bright, multicoloured light-emitting diodes based on quantum dots," Nat. Photonics **1**, 717–722 (2007).
5. D. Psaltis, S. R. Quake, and C. Yang, "Developing optofluidic technology through the fusion of microfluidics and optics," Nature **442**, 381–386 (2006).
6. H. Schmidt and A. R. Hawkins, "The photonic integration of non-solid media using optofluidics," Nat. Photonics **5**, 598–604 (2011).
7. Y. Yang, A. Liu, L. Lei, L. Chin, C. Ohl, Q. Wang, and H. Yoon, "A tunable 3D optofluidic waveguide dye laser via two centrifugal Dean flow streams," Lab Chip **11**, 3182–3187 (2011).
8. Y. Yang, A. Liu, L. Chin, X. Zhang, D. Tsai, C. Lin, C. Lu, G. Wang, and N. Zheludev, "Optofluidic waveguide as a transformation optics device for lightwave bending and manipulation," Nat. Commun. **3**, 651 (2012).
9. R. M. Vazquez, G. Nava, M. Veglione, T. Yang, F. Bragheri, P. Minzioni, E. Bianchi, M. Di Tano, I. Chiodi, and R. Osellame, "An optofluidic constriction chip for monitoring metastatic potential and drug response of cancer cells," Integr. Biol. **7**, 477–484 (2015).
10. M. Schadt, H. Seiberle, and A. Schuster, "Optical patterning of multi-domain liquid-crystal displays with wide viewing angles," Nature **381**, 212–215 (1996).
11. F. P. Schäfer, *Dye Lasers* (Springer, 2013).
12. C. K. Chan, H. Peng, G. Liu, K. McIlwrath, X. F. Zhang, R. A. Huggins, and Y. Cui, "High-performance lithium battery anodes using silicon nanowires," Nat. Nanotechnol. **3**, 31–35 (2008).
13. D. B. Wolfe, R. S. Conroy, P. Garstecki, B. T. Mayers, M. A. Fischbach, K. E. Paul, M. Prentiss, and G. M. Whitesides, "Dynamic control of liquid-core/liquid-cladding optical waveguides," Proc. Natl. Acad. Sci. USA **101**, 12434–12438 (2004).
14. R. Melikov, D. A. Press, B. G. Kumar, I. B. Dogru, S. Sadeghi, M. Chirea, İ. Yılgör, and S. Nizamoglu, "Silk-hydrogel lenses for light-emitting diodes," Sci. Rep. **7**, 7258 (2017).
15. C.-W. Sher, C.-H. Lin, H.-Y. Lin, C.-C. Lin, C.-H. Huang, K.-J. Chen, J.-R. Li, K.-Y. Wang, H.-H. Tu, and C.-C. Fu, "A high quality liquid-type quantum dot white light-emitting diode," Nanoscale **8**, 1117–1122 (2016).
16. S. Y. Lee, K.-I. Park, C. Huh, M. Koo, H. G. Yoo, S. Kim, C. S. Ah, G. Y. Sung, and K. J. Lee, "Water-resistant flexible GaN LED on a liquid crystal polymer substrate for implantable biomedical applications," Nano Energy **1**, 145–151 (2012).
17. M. Lu, X. Bai, Y. Lin, C. Ji, H. Wu, C. Ruan, W. Gao, Y. Wang, and Q. Du, "Liquid-type AgInS 2/ZnS quantum dot-based warm white light-emitting diodes," Chem. Phys. Lett. **661**, 228–233 (2016).
18. Y. Wang, X. Bai, T. Wang, L. Yan, T. Zhang, Y. Zhang, and W. Y. William, "Efficient near-infrared light-emitting diodes based on liquid PbSe quantum dots," Nanotechnology **28**, 215703 (2017).
19. M. A. Hines and P. Guyot-Sionnest, "Synthesis and characterization of strongly luminescing ZnS-capped CdSe nanocrystals," J. Phys. Chem. **100**, 468–471 (1996).
20. B. O. Dabbousi, J. Rodriguez-Viejo, F. V. Mikulec, J. R. Heine, H. Mattoussi, R. Ober, K. F. Jensen, and M. G. Bawendi, "(CdSe) ZnS core-shell quantum dots: synthesis and characterization of a size series of highly luminescent nanocrystallites," J. Phys. Chem. B **101**, 9463–9475 (1997).
21. X. Peng, M. C. Schlamp, A. V. Kadavanich, and A. P. Alivisatos, "Epitaxial growth of highly luminescent CdSe/CdS core/shell nanocrystals with photostability and electronic accessibility," J. Am. Chem. Soc. **119**, 7019–7029 (1997).
22. J. S. Steckel, J. P. Zimmer, S. Coe-Sullivan, N. E. Stott, V. Bulović, and M. G. Bawendi, "Blue luminescence from (CdS) ZnS core–shell nanocrystals," Angew. Chem. (Int. Ed.) **43**, 2154–2158 (2004).
23. J. S. Steckel, P. Snee, S. Coe-Sullivan, J. P. Zimmer, J. E. Halpert, P. Anikeeva, L. A. Kim, V. Bulovic, and M. G. Bawendi, "Color-saturated green-emitting QD-LEDs," Angew. Chem. (Int. Ed.) **45**, 5796–5799 (2006).
24. E. Jang, S. Jun, H. Jang, J. Lim, B. Kim, and Y. Kim, "White-light-emitting diodes with quantum dot color converters for display backlights," Adv. Mater. **22**, 3076–3080 (2010).
25. H. Zhang, S. Chen, and X. W. Sun, "Efficient red/green/blue tandem quantum-dot light-emitting diodes with external quantum efficiency exceeding 21%," ACS Nano **12**, 697–704 (2018).
26. H. Li, K. Wu, J. Lim, H.-J. Song, and V. I. Klimov, "Doctor-blade deposition of quantum dots onto standard window glass for low- loss large-area luminescent solar concentrators," Nat. Energy **1**, 16157 (2016).
27. F. Meinardi, A. Colombo, K. A. Velizhanin, R. Simonutti, M. Lorenzon, L. Beverina, R. Viswanatha, V. I. Klimov, and S. Brovelli, "Large-area luminescent solar concentrators based on 'Stokes-shift-engineered' nanocrystals in a mass-polymerized PMMA matrix," Nat. Photonics **8**, 392–399 (2014).
28. S. Sadeghi, H. Bahmani Jalali, R. Melikov, B. Ganesh Kumar, M. Mohammadi Aria, C. W. Ow-Yang, and S. Nizamoğlu, "Stokes-shift-engineered indium phosphide quantum dots for efficient luminescent solar concentrators," ACS Appl. Mater. Interfaces **10**, 12975–12982 (2018).
29. B. N. Pal, Y. Ghosh, S. Brovelli, R. Laocharoensuk, V. I. Klimov, J. A. Hollingsworth, and H. Htoon, "'Giant'CdSe/CdS core/shell nanocrystal quantum dots as efficient electroluminescent materials: strong influence of shell thickness on light-emitting diode performance," Nano Lett. **12**, 331–336 (2011).
30. Y. Chen, J. Vela, H. Htoon, J. L. Casson, D. J. Werder, D. A. Bussian, V. I. Klimov, and J. A. Hollingsworth, "'Giant' multishell CdSe nanocrystal quantum dots with suppressed blinking," J. Am. Chem. Soc. **130**, 5026–5027 (2008).
31. T. A. Klar, T. Franzl, A. L. Rogach, and J. Feldmann, "Super-efficient exciton funneling in layer-by-layer semiconductor nanocrystal structures," Adv. Mater. **17**, 769–773 (2005).
32. S. Nizamoglu and H. V. Demir, "Resonant nonradiative energy transfer in CdSe/ZnS core/shell nanocrystal solids enhances hybrid white light emitting diodes," Opt. Express **16**, 13961–13968 (2008).
33. H. M. Haverinen, R. A. Myllylä, and G. E. Jabbour, "Inkjet printing of light emitting quantum dots," Appl. Phys. Lett. **94**, 073108 (2009).
34. A. Kshirsagar, S. Pickering, J. Xu, and J. Ruzyllo, "Light emitting diodes formed using mist deposition of colloidal solution of CdSe nanocrystalline quantum dots," ECS Trans. **35**, 71–77 (2011).
35. J. Lim, S. Jun, E. Jang, H. Baik, H. Kim, and J. Cho, "Preparation of highly luminescent nanocrystals and their application to light-emitting diodes," Adv. Mater. **19**, 1927–1932 (2007).
36. S. Jun and E. Jang, "Interfused semiconductor nanocrystals: brilliant blue photoluminescence and electroluminescence," Chem. Commun., 4616–4618 (2005).
37. E. F. Schubert, T. Gessmann, and J. K. Kim, *Light Emitting Diodes* (Wiley, 2005).

38. C. Pu and X. Peng, "To battle surface traps on CdSe/CdS core/shell nanocrystals: shell isolation versus surface treatment," J. Am. Chem. Soc. **138**, 8134–8142 (2016).
39. R. Melikov, D. A. Press, B. Ganesh Kumar, S. Sadeghi, and S. Nizamoglu, "Unravelling radiative energy transfer in solid-state lighting," J. Appl. Phys. **123**, 023103 (2018).
40. Y. Narukawa, M. Ichikawa, D. Sanga, M. Sano, and T. Mukai, "White light emitting diodes with super-high luminous efficacy," J. Phys. D **43**, 354002 (2010).
41. J. C. McDonald and G. M. Whitesides, "Poly (dimethylsiloxane) as a material for fabricating microfluidic devices," Acc. Chem. Res. **35**, 491–499 (2002).
42. L. Qian, Y. Zheng, J. Xue, and P. H. Holloway, "Stable and efficient quantum-dot light-emitting diodes based on solution- processed multilayer structures," Nat. Photonics **5**, 543–548 (2011).
43. C. Luk, L. Tang, W. Zhang, S. Yu, K. Teng, and S. Lau, "An efficient and stable fluorescent graphene quantum dot-agar composite as a converting material in white light emitting diodes," J. Mater. Chem. **22**, 22378–22381 (2012).
44. H. Wang, K.-S. Lee, J.-H. Ryu, C.-H. Hong, and Y.-H. Cho, "White light emitting diodes realized by using an active packaging method with CdSe/ZnS quantum dots dispersed in photosensitive epoxy resins," Nanotechnology **19**, 145202 (2008).
45. V. Wood, M. J. Panzer, J. Chen, M. S. Bradley, J. E. Halpert, M. G. Bawendi, and V. Bulović, "Inkjet-printed quantum dot-polymer composites for full-color ac-driven displays," Adv. Mater. **21**, 2151–2155 (2009).
46. Y.-S. Su, C.-C. Hsiao, and S.-R. Chung, "CdSe white quantum dots-based white light-emitting diodes with high color rendering index," Proc. SPIE **9954**, 99540B (2016).
47. S. J. Yang, J. H. Oh, S. Kim, H. Yang, and Y. R. Do, "Realization of InP/ZnS quantum dots for green, amber and red down- converted LEDs and their color-tunable, four-package white LEDs," J. Mater. Chem. C **3**, 3582–3591 (2015).
48. H.-Y. Lin, S.-W. Wang, C.-C. Lin, K.-J. Chen, H.-V. Han, Z.-Y. Tu, H.-H. Tu, T.-M. Chen, M.-H. Shih, and P.-T. Lee, "Excellent color quality of white-light-emitting diodes by embedding quantum dots in polymers material," IEEE J. Sel. Top. Quantum Electron. **22**, 35–41 (2016).
49. H. Shen, Q. Lin, H. Wang, L. Qian, Y. Yang, A. Titov, J. Hyvonen, Y. Zheng, and L. S. Li, "Efficient and bright colloidal quantum dot light-emitting diodes via controlling the shell thickness of quantum dots," ACS Appl. Mater. Interfaces **5**, 12011–12016 (2013).
50. K.-J. Chen, C.-C. Lin, H.-V. Han, C.-Y. Lee, S.-H. Chien, K.-Y. Wang, S.-H. Chiu, Z.-Y. Tu, J.-R. Li, and T.-M. Chen, "Wide-range correlated color temperature light generation from resonant cavity hybrid quantum dot light-emitting diodes," IEEE J. Sel. Top. Quantum Electron. **21**, 23–29 (2015).
51. Y.-K. Kim, K.-C. Choi, Y.-K. Baek, and P.-W. Shin, "Enhanced luminescence stability of quantum dot-based inorganic nanocomposite particles for white-light-emitting diodes," Mater. Lett. **124**, 129–132 (2014).
52. P.-H. Chuang, C. C. Lin, and R.-S. Liu, "Emission-tunable CuInS2/ZnS quantum dots: structure, optical properties, and application in white light-emitting diodes with high color rendering index," ACS Appl. Mater. Interfaces **6**, 15379–15387 (2014).
53. X. Yuan, R. Ma, W. Zhang, J. Hua, X. Meng, X. Zhong, J. Zhang, J. Zhao, and H. Li, "Dual emissive manganese and copper co-doped Zn-In–S quantum dots as a single color-converter for high color rendering white-light-emitting diodes," ACS Appl. Mater. Interfaces **7**, 8659–8666 (2015).
54. S. H. Park, A. Hong, J.-H. Kim, H. Yang, K. Lee, and H. S. Jang, "Highly bright yellow-green-emitting CuInS2 colloidal quantum dots with core/shell/shell architecture for white light-emitting diodes," ACS Appl. Mater. Interfaces **7**, 6764–6771 (2015).
55. B. Chen, H. Zhong, M. Wang, R. Liu, and B. Zou, "Integration of CuInS 2-based nanocrystals for high efficiency and high colour rendering white light-emitting diodes," Nanoscale **5**, 3514–3519 (2013).
56. X. Yuan, J. Hua, R. Zeng, D. Zhu, W. Ji, P. Jing, X. Meng, J. Zhao, and H. Li, "Efficient white light emitting diodes based on Cu-doped ZnInS/ZnS core/shell quantum dots," Nanotechnology **25**, 435202 (2014).
57. J. Ryckaert, A. Correia, M. D. Tessier, D. Dupont, Z. Hens, P. Hanselaer, and Y. Meuret, "Selecting the optimal synthesis parameters of InP/CdxZn 1–x Se quantum dots for a hybrid remote phosphor white LED for general lighting applications," Opt. Express **25**, A1009–A1022 (2017).
58. H. C. Yoon, H. Kang, S. Lee, J. H. Oh, H. Yang, and Y. R. Do, "Study of perovskite QD down-converted LEDs and six-color white LEDs for future displays with excellent color performance," ACS Appl. Mater. Interfaces **8**, 18189–18200 (2016).
59. R. Melikov, Simulation Codes for White Light-Emitting Diodes (figshare, 2018), https://figshare.com/s/1f5950313347f81bba57.